

# Journal of Materials Chemistry B

Accepted Manuscript



This is an *Accepted Manuscript*, which has been through the Royal Society of Chemistry peer review process and has been accepted for publication.

*Accepted Manuscripts* are published online shortly after acceptance, before technical editing, formatting and proof reading. Using this free service, authors can make their results available to the community, in citable form, before we publish the edited article. We will replace this *Accepted Manuscript* with the edited and formatted *Advance Article* as soon as it is available.

You can find more information about *Accepted Manuscripts* in the [Information for Authors](#).

Please note that technical editing may introduce minor changes to the text and/or graphics, which may alter content. The journal's standard [Terms & Conditions](#) and the [Ethical guidelines](#) still apply. In no event shall the Royal Society of Chemistry be held responsible for any errors or omissions in this *Accepted Manuscript* or any consequences arising from the use of any information it contains.

## The effect of PEGylation on the stimulation of IL-1 $\beta$ by gold (Au) nanoshell/silica core nanoparticles

Hai T. Nguyen<sup>a</sup> and Hong Shen<sup>b\*</sup>

Received 00th January 20xx,  
Accepted 00th January 20xx

DOI: 10.1039/x0xx00000x

www.rsc.org/

Au nanoshell/silica core (GNS) nanoparticles have been used for the photothermal ablation of tumors and imaging, and have recently reached clinical trials. In this study, we compared the ability of bare (GNS) and PEGylated Au nanoshell/silica core (PEG-GNS) nanoparticles in stimulating the production of IL-1 $\beta$  in both macrophage cell lines. GNS particles formed large aggregates while PEG-GNS particles did not in cell culture medium. Correspondingly, GNS particles induced the production of IL-1 $\beta$  while PEG-GNS did not in THP-1 macrophage cell line. Corroborating with *in vitro* results, GNS induced a significant level of neutrophil influx in peritoneal cavity, and PEG-GNS reduced the level four times. The density of PEG on particle surface has little effect on both the induction of IL-1 $\beta$  and neutrophil influx by PEG-GNS. The ability of induction and scavenging reactive oxygen species (ROS) by GNS and PEG-GNS particles were also assessed. We demonstrated that GNS was able to induce and scavenge ROS while PEG-GNS was not. The excess of ROS induced by GNS potentially caused the activation of inflammasomes, and thus the secretion of IL-1 $\beta$ . Our finding in the reduction IL-1 $\beta$  production by PEGylation of nanoparticles has implications in other particulates used for drug delivery, imaging and therapy.

### Introduction

Au nanoshell/silica core (GNS) nanoparticles have a broad spectrum of applications due to their unique tunable plasmon resonance.<sup>1</sup> One of primary applications is laser-induced photothermal therapy, particularly for targeting cancer cells due to their passive accumulation at vascularized tumors<sup>2-5</sup>. Circulating nanoparticles have been shown to accumulate in other healthy organs as well, such as the liver, kidneys, spleen, and lungs<sup>6</sup>. In those organs, there exist abundant macrophages and other phagocytes that tend to engulf nanoparticles encountered.

GNS for cancer treatment and imaging has been considered relatively safe and biocompatible.<sup>7-9</sup> In recent years, particulates, such as micro- and nano- sized silica particles,<sup>10-12</sup> asbestos,<sup>10</sup> aluminum hydroxide,<sup>11</sup> and crystal uric acid<sup>13</sup>, have been shown to activate an intracellular sensor, NACHT, LRR and PYD domains-containing protein 3 (NALP3) inflammasome, in phagocytes. NALP3 Inflammasome is a protein complex consisting of apoptosis-associated speck protein with a caspase and recruitment domain (ASC) and caspase-1. NALP3 acts as a scaffold protein, and ASC bridges NALP3 to caspase-1 for its activation. The activated caspase-1 then cleaves precursors of proinflammatory cytokines, such as pro-IL-1 $\beta$ , to IL-1 $\beta$ .<sup>14</sup> The release of IL-1 $\beta$  into extracellular space triggers neutrophilic inflammatory responses. Several diseases, including silicosis, gout, asbestosis, type II diabetes mellitus, are involved in the pathway of NALP3-IL-1 $\beta$ . IL-1 $\beta$  has been responsible for many other disorders, which are extensively reviewed by

Schroder and Tschopp<sup>15</sup>.

It has been suggested that silica particles induced reactive oxygen species (ROS) that was responsible for the activation of NALP3 inflammasome.<sup>12</sup> Au nanoparticles, however, have been shown to be capable of scavenging ROS.<sup>16</sup> Would GNS nanoparticles induce ROS and IL-1 $\beta$ ? In order to enhance their circulation time, poly(ethylene glycol) (PEG) has been used for modifying the surface of GNS nanoparticles.<sup>17</sup> How would PEGylation affect the generation and scavenging ROS by Au nanoshell/silica core nanoparticles? Would PEG attenuate or enhance the ability of GNS nanoparticles in inducing the secretions of IL-1 $\beta$ ?

In this study, we set out to address these questions. We show that GNS nanoparticles, currently involved in clinical trials, were able to induce IL-1 $\beta$  secretions and neutrophil influx *in vivo*; PEGylation reduced the level of IL-1 $\beta$  by macrophage cell lines and the recruitment of neutrophils *in vivo*. Our results suggest that GNS nanoparticles mediated-inflammation can occur in various organs that are not being targeted for nanoshell enabled photothermal therapy or imaging. Neutrophilic inflammation due to the generation of IL-1 $\beta$  by GNS nanoparticles should be carefully assessed. Surface modification of GNS nanoparticles or other nanoparticles by PEGylation can potentially reduce the probability of stimulating the production of ROS and IL-1 $\beta$ .

<sup>a</sup> Department of Chemical Engineering, University of Washington, Box 351750, Seattle, WA 98195, USA

<sup>b</sup> Elsa Biologics, LLC, Box 25725, Seattle, WA 98165, USA

\*Corresponding author. Tel.: +1 206 491 3482. E-mail address: hong.shen@elsa-biologics.com

Supplementary Information (ESI) available: [The secretions of IL-1 $\beta$  by THP-1 cells treated with silica NP]. See DOI: 10.1039/x0xx00000x

## Results and Discussion

### Characterization of nanoparticles

Three types of nanoparticles, including GNS, PEG-GNS and silica nanoparticles (Silica NP), were used in this study. GNS consisted of a silica core of  $119 \pm 11$  nm in diameter and a 17 nm-thick of Au shell (Figure 1A). Silica NP, the same as the silica core in GNS, exhibited positive charge with the zeta potential of 40 mV (Figure 1A, B and D). PEG-GNS showed an increase in hydrodynamic diameter up to 30 nm (Figure 1B) and in zeta potential to nearly neutral when the concentration of PEG-SH in coating reaction increased (Figure 1D). These results were consistent with previous studies that showed PEGylated nanoparticles exhibited an increase in hydrodynamic diameter and neutralization of surface charge compared to their non-PEGylated ones.<sup>18</sup> The thickness of PEG corona on GNS was determined by calculating the difference of hydrodynamic diameter between GNS and PEG-GNS (Figure 1C). Marsh et. al suggest that PEG adopts from "mushroom" to "brush" conformations categorized based on the thickness of PEG coating.<sup>19</sup> We compared our estimations with those by Marsh et. al.<sup>19</sup> For PEG-GNS in our study, lower than 5 nM of PEG-SH in the coating reaction adopted a mushroom conformation while concentrations above 5 nM resulted in a brush conformation.

Both GNS and PEG-GNS nanoparticles used in this study exhibited similar dimensions (Figure 1A and B) and optical properties (Figure 1E) as in previous *in vivo* and *in vitro* studies.<sup>2, 3, 20-25</sup>

### Morphological changes of nanoparticles and macrophages

After 24 h-incubation with cells at 37°C, GNS formed aggregates, the size of which increased as the concentration of GNS increased (Figure 2, top row). The PEG-GNS was well dispersed and formed small clusters (Figure 2, middle row). At low concentrations of GNS, cells appeared the similar morphology to control cells without particles. At high concentrations (> 3 mg/ml) of GNS, cells formed large clusters around the aggregates of GNS (Figure 2, top row). In the presence of PEG-GNS, cells did not exhibit significant morphological changes at the range of concentrations (0.1 ~ 5 mg/ml) we investigated (Figure 2, middle row). Cells formed clusters in the presence of both Silica NP and silica microparticles (Silica  $\mu$ P) (Figure 2, bottom row).

### Induction of secretions of IL-1 $\beta$ by nanoparticles

Recent studies suggest that particulates such as silica particles and asbestos can activate NALP3 inflammasome and induce the cleavage of pro-IL-1 and subsequent IL-1 $\beta$  secretions.<sup>10, 11, 13, 26</sup> We examined whether GNS, PEG-GNS and silica NP stimulated the secretions of IL-1 $\beta$  by THP-1, a human macrophage-like cell line (Figure 3). THP-1 cells have been shown to respond to a variety of well-documented inflammasome-inducers.<sup>27-29</sup> THP-1 cells were first treated with lipopolysaccharide (LPS) to induce pro-IL-1 $\beta$ . Upon the stimulation of inflammasomes, pro-IL-1 $\beta$  is cleaved into IL-1 $\beta$ , which is secreted from cells. The stimulation of inflammasomes can therefore be assessed by the secretion of IL-1 $\beta$  in THP-1 cells.

Some studies treated THP-1 first with Phorbol-12-myristate-13-acetate (PMA) and then LPS. Using silica particles, we compared the IL-1 $\beta$  secretions by THP-1 cells treated with LPS only or LPS and PMA. We did not observe significant difference between two pre-treatments (Supplemental Figure 1). THP-1 cells without PMA treatment were more sensitive to a low concentration of silica particles and secrete higher level of IL-1 $\beta$  compared to cells treated with both PMA and LPS. It has also been suggested that PMA

treatment can up-regulate some genes in THP-1 cells that overwhelm gene expression changes by stimuli of interest.<sup>30</sup> Therefore, in this study, we treated THP-1 cells with LPS only.

As shown in Figure 3 A, GNS yielded a statistically significant higher level of IL-1 $\beta$  ( $p < 0.05$ ) at or greater than 3 mg/ml nanoparticles compared to cells without particles, and the level of IL-1 $\beta$  increased as concentrations of particles increased. Silica NP at the same either mass concentration (Figure 3A) or number of particles per cells (Figure 3B) as GNS particles induced nearly 6 fold higher level of IL-1 $\beta$ . When the concentration of silica NP was greater than 2 mg/ml, the level of IL-2 $\beta$  started to level off because of cell death. PEGylation reduced the level of IL-1 $\beta$  induced by GNS (Figure 3A). In summary, the ability of the same mass concentration of nanoparticles in stimulating the inflammasomes followed the order: silica NP > GNS > PEG-GNS nanoparticles.

We subsequently examined whether the coverage of PEG would affect the induction of IL-1 $\beta$  by PEG-GNS (Figure 3C). PEG coating reduced the level of IL-1 $\beta$  induced by GNS significantly at as low as 0.01 or 0.05 mM PEG-GNS used in the coating reaction. Based on the zeta potential measurement (Figure 1D), the coverage of PEG on GNS at these two concentrations was low. As the coverage further increased (PEG-SH concentration was at 0.1 nM), the level of IL-1 $\beta$  decreased to the same level as untreated cells. From Figure 1D, zeta potential increased from -45 mV to -30 mV when the coating concentration of PEG-SH changed from 0.05 to 0.1 nM. It indicated that PEG coverage was significantly increased. As the concentration of PEG-SH further increased, there was no significant change in the level of IL-1 $\beta$ , although zeta potential continued increasing. These results suggest a threshold of PEG coverage may be required in order to completely abolish the induction of IL-1 $\beta$  by a type of particles, i.e. GNS.

### Recruitment of neutrophils *in vivo*

IL-1 $\beta$  mediates the influx of neutrophils *in vivo* by the induction of neutrophil-attracting chemokines and the up-regulation of adhesion molecules by the vasculature.<sup>31</sup> It also prolongs the survival of neutrophils. As a result, it increases the number of neutrophils locally. We then assessed whether GNS and PEG-GNS could induce the influx of neutrophils into the peritoneal cavity of mice, which contains a large quantity of macrophages, by injecting different amounts of particles into the cavity (Figure 4). Two surface molecules, Lys-6B.2(7/4) and Lys-6G, were used to identify the neutrophils. Alum, a known agent that induces the neutrophil influx, was used as positive control and to determine the gating of Lys-6B.2(7/4) and Lys-6G positive cells (Figure 4A). Consistent with previous studies, Alum recruited a high level ( $8 \times 10^6$  cells/2.5 mg Alum) of neutrophils into peritoneal cavity.<sup>11</sup>

We chose a dose range of GNS or PEG-GNS commonly used *in vivo* studies.<sup>2-4, 32</sup> Sixteen hours later, the number of neutrophils in peritoneal lavage was assessed (Figure 4B). GNS induced the neutrophil influx in a dose-dependent manner, and PEGylation reduced the level of neutrophil influx significantly. Consistent with our observations of IL-1 $\beta$  secretions by THP-1 cells, the density of PEG on the surface of GNS did not affect the level of neutrophil influx significantly although it was reproducibly observed that the higher PEG coverage reduced the influx of neutrophils at a higher degree. We would also like to note that PEGylation of GNS induced a much lower level of neutrophil influx in comparison with bare

GNS-treated mice but did not completely abolish the neutrophil influx in comparison with PBS-treated mice.

#### Generation of ROS by nanoparticles

It has been shown that many particulates, such as silica particles or uric acid, induce IL-1 $\beta$  through the ROS-dependent activation of NALP3 inflammasome.<sup>10</sup> The ROS releases thioredoxin (TRX)-interacting protein (TXNIP) from TRX, and the released TXNIP binds and activates inflammasome.<sup>33</sup> We subsequently assessed intracellular ROS levels induced by different nanoparticles by a ROS fluorescent probe, H2DCFDA (Figure 5A – D).

Cells exposed to a given concentration of soluble H<sub>2</sub>O<sub>2</sub> and silica microparticles (Silica  $\mu$ P) were used as controls. We monitored the fluorescence change for 2 h. The fluorescence of oxidized H2DCFDA, i.e. DCF, leveled off after 1 hour for all the particle groups and soluble H<sub>2</sub>O<sub>2</sub> except high concentrations of silica NP and  $\mu$ P. For clarification, we compared all the groups at 100 min (Figure 5E). As expected, intracellular level of H<sub>2</sub>O<sub>2</sub> linearly increased as extracellular concentration of H<sub>2</sub>O<sub>2</sub> increased. Silica  $\mu$ P generated a significant level of ROS as demonstrated in previous studies.<sup>12</sup> Silica NP also generated a significant level of intracellular ROS, which increased as the mass concentration of particles increased. Both GNS and PEG-GNS did not yield a significantly higher level of intracellular ROS in comparison with cells without any treatments.

#### Scavenging and fluorescent quenching by Au nanoparticles

GNS particles at the concentration greater than 3 mg/ml instigated a low, but significantly higher level of IL-1 $\beta$  in comparison to control cells *in vitro* (Figure 3A) and GNS particles induced neutrophil influx in peritoneal cavity (Figure 4B). The signal of DCF of cells treated by GNS and PEG-GNS nanoparticles was unexpectedly lower than or at most similar to untreated cells.

Two questions were raised: do GNS or PEG-GNS nanoparticles not generate ROS at all or is the generated ROS scavenged by them? Do Au nanoparticles quench the fluorescence of DCF? We first tested whether Au nanoparticles acted as the scavenger of ROS. A known concentration of H<sub>2</sub>O<sub>2</sub> was reacted with both GNS and PEG-GNS nanoparticles for 45 min followed by the complete removal of Au nanoparticles. The residual of H<sub>2</sub>O<sub>2</sub> was detected by H<sub>2</sub>DCFDA. As shown in Figure 6A, in the presence of GNS particles, the level of H<sub>2</sub>O<sub>2</sub> was reduced and the decrease was proportional to the amount of GNS nanoparticles. In contrast, PEG-GNS resulted in little change in the level of H<sub>2</sub>O<sub>2</sub> (Figure 6B). These results demonstrate that GNS particles can decompose H<sub>2</sub>O<sub>2</sub> while PEG-GNS particles cannot.

The broad absorption spectrum of both GNS and PEG-GNS particles (Figure 1E) suggested that they could potentially quench the fluorescence of DCF, which was excited at 490 nm and emitted at 536 nm. We tested this possibility by first oxidizing H<sub>2</sub>DCFDA with a given concentration of H<sub>2</sub>O<sub>2</sub> and then assessed the fluorescence intensity of DCF in the presence or absence of GNS or PEG-GNS. As shown in Figure 7, both GNS and PEG-GNS quenched the fluorescence of DCF at a concentration dependent manner. In the presence of 1 mg/ml of particles, the fluorescence of DCF was reduced 6 times.

GNS and PEG-GNS exhibited a similar degree of quenching at the same concentration of particles while only GNS was able to scavenge ROS significantly. These results suggest the intracellular DCF signals (Figure 5) were not directly correlated with the amount of ROS produced by cells exposed to either GNS or PEG-GNS. At low concentrations of particles, intracellular DCF signal induced by PEG-

GNS was lower or similar to untreated cells while that induced by GNS was lower than untreated cells. The DCF signals due to the generation of ROS by either PEG-GNS or GNS were quenched or scavenged. This indicated that both PEG-GNS and GNS generated a low level of ROS at low concentrations of particles. At high concentrations (> 3 mg/ml), intracellular DCF signals for PEG-GNS-treated cells was completely diminished which suggests that the level of ROS generated was still low, and the DCF signal due to ROS was completely quenched by the high concentration of PEG-GNS. On the contrary, intracellular DCF in GNS-treated cells was similar to untreated cells, though a much significantly higher level of quenching and scavenging was expected than that at low concentrations of particles. This indicates that GNS at high concentrations induced a much higher level of ROS than PEG-GNS and than at the low concentrations of GNS. The excess of ROS, which was not decomposed by GNS nanoparticles, was expected to contribute to the activation of NALP3 inflammasomes and instigate the secretions of IL-1 $\beta$ .

## Discussion

GNS are currently utilized in clinical trials for cancer treatment.<sup>34</sup> The components of these particles, silica and Au, are considered to be both biocompatible and nontoxic, and are used in various applications in medicine.<sup>8</sup> In this study, we have assessed the ability of GNS, PEGylated GNS (PEG-GNS) and silica core nanoparticles (Silica NP) to induce the production of proinflammatory cytokines IL-1 $\beta$  (Figure 3). Our results demonstrate that bare GNS induced significantly higher levels of IL-1 $\beta$  by THP-1 macrophages at concentrations greater than 3 mg/ml compared to untreated cells while PEG-GNS did not (Figure 3); silica core nanoparticles yielded about 6 times higher level of IL-1 $\beta$  by THP-1 macrophages than GNS at the same mass concentration or the number of particles per cells (Figure 3A-B). Surprisingly, a significant level of neutrophil recruitment was observed even at the medium to low concentration range of GNS that used for *in vivo* photothermal cancer treatment.<sup>2,4,32,35</sup> PEG-GNS reduced but did not abolish the influx of neutrophils. We tried to detect the IL-1 $\beta$  in blood and in peritoneal lavage by ELISA. The level was low to undetectable. It is likely due to the dilution in blood (about 2 ml) or lavage washes (about 10 ml). The detection limit of ELISA is 20 pg/ml. The minimal concentration of IL-1 $\beta$  in blood and lavages must be 40 or 200 pg/ml, respectively, to be detected. This level of IL-1 $\beta$  is sufficient to induce the recruitment of neutrophils.

It has recently been suggested that the ROS induced by particulates, such as silica NP and  $\mu$ P and crystal uric acid, activates NALP3 inflammasome, which cleaves pro-IL-1 $\beta$  into secretory form of IL-1 $\beta$ .<sup>10,12,36,37</sup> Intracellular ROS was detected by H2DCFDA in this study. For silica particles, the generation of IL-1 $\beta$  was correlated with the intensity of DCF and the level of ROS, which is consistent with previous findings.<sup>12,38</sup> The correlation of DCF signal, ROS level and IL-1 $\beta$  generation induced by GNS and PEG-GNS became less apparent due to the quenching and scavenging effects of these particles (Figure 6 and 7). Based on our observations (Figure 5 - 7), PEG-GNS did not seem to induce a significant level ROS (Figure 5B), and the reduced signal of DCF compared to untreated cells was possibly due to the quenching effect by particles (Figure 7). GNS did induce ROS at high concentrations (> 3 mg/ml), though the scavenging (Figure 6A) reduced the intracellular level of ROS and the quenching effect decreased the signal of DCF (Figure 7). The

scavenging effect of GNS might explain that GNS was less active in stimulating the secretion of IL-1 $\beta$  than silica NP ( $p < 0.05$ ) (Figure 3).

ROS can be generated due to frustrated phagocytosis, which occurs when particles cannot be internalized by cells. Frustrated phagocytosis is considered to activate the NADPH oxidase-mediated pathway to generate ROS.<sup>39</sup> Zhou and colleagues have recently demonstrated that mitochondria, in response to the insult from particulates such as silica and MSU crystals, can generate ROS as well.<sup>37</sup> GNS nanoparticles formed aggregates in cell culture, which became more severe at the high mass concentrations. Macrophages formed clusters and attempted to engulf the aggregated GNS (Figure 2, top row). In contrast, PEG-GNS nanoparticles remained dispersed and formed rather small aggregates even at high concentrations; cells did not cluster around these aggregates and attempt to engulf them (Figure 2, middle row). Zhang et al. have demonstrated that fumed silica NP, which forms chainlike structures and cannot be internalized by cells, activates inflammasomes.<sup>40</sup> The fumed silica nanostructure formed on the surface of the cells in the study are similar to aggregated GNS in this study. They propose that fumed silica NP causes the damage of cell membrane via hydrogen-bonding interactions. As a result, cells produce ROS either through NADPH oxidase pathway or from strained siloxane rings on fumed silica NP. GNS can scavenge ROS (Figure 6). GNS itself unlikely acts as the source of ROS. We speculate that the induction of ROS by GNS was most likely due to frustrated phagocytosis through NADPH oxidase-mediated pathway or other pathways. The detailed mechanisms require further elucidations.

GNS particles injected intravenously for cancer photothermal therapy accumulates in the liver, kidney, spleen, and lungs in addition to the targeted tumor sites.<sup>6</sup> High levels of accumulation in those organs can expose phagocytes, such as macrophages, to an environment containing a high concentration of particles. In such cases, the stimulation of IL-1 $\beta$  secretions likely occurs and leads to a cascade of inflammatory responses in untargeted organs. Chronic inflammation at untargeted sites can compromise the treatment of cancers and cause severe side effects.<sup>41,42</sup> GNS nanoparticles are often PEGylated for *in vivo* applications.<sup>3,6</sup> The PEGylation provides the steric repulsion to reduce aggregation of nanoparticles as well as protein absorption.<sup>17</sup> Our results suggest that PEGylation possibly attenuates the ability of GNS in stimulating ROS due to the frustrated phagocytosis by reducing the amount of aggregation that occurs (Figure 2). On the other hand, PEGylation mitigated the scavenging effect of ROS by GNS. Careful optimization of parameters of PEGylation would maximize the therapeutic effects of GNS while reducing the unwanted inflammatory responses. Our studies investigated the effect of PEG and its surface coverage on the reduction of the neutrophil influx of GNS nanoparticles. The finding can be extended to other particles (i.e. gold nanorods, silica nanoparticles) that are used for either therapy or imaging.

## Experimental

### Materials

Tetraethyl orthosilicate, ammonia, (3-Aminopropyl) trimethoxysilane, gold (III) chloride hydrate, sodium bicarbonate, tetrakis(hydroxymethyl)phosphonium chloride solution, sodium chloride, dihydrorhodamine 123, dichlorodihydrofluorescein, and sodium carbonate were obtained from Sigma-Aldrich (St. Louis, MO) and used as received. Carbon monoxide gas was obtained from

Praxair (Danbury, CT). Cell culture supplies were obtained from Invitrogen (Carlsbad, CA). Min-U-Sil-15 was kindly provided by U.S. Silica (Berkeley Springs, WV). Enzyme-linked immunosorbent assay (ELISA) reagents including primary and secondary antibodies, streptavidin-horse radish peroxidase (SA-HRP), and 3,3',5,5'-tetramethylbenzidine (TMB) were obtained from eBiosciences (San Diego, CA).

### Cell Culture

THP-1 cells (ATCC) were maintained in Roswell Park Memorial Institute (RPMI) 1640 media supplemented with 10% fetal bovine serum (FBS), 2 mM L-glutamine, 1mM sodium pyruvate, 10 mM (4-(2-hydroxyethyl)-1-piperazineethanesulfonic acid) (HEPES), 50  $\mu$ M 2-mercaptoethanol (2-ME), and 1.5 g/L glucose. Cells were maintained at 37  $^{\circ}$ C and 5% CO<sub>2</sub>, and kept at a concentration of between 4 and 8  $\times 10^5$  cells/ml. Passages between 6 and 16 were used for this study.

### Fabrication of nanoparticles

Silica core nanoparticles (Silica NP) and Au nanoshell/silica core nanoparticles (GNS) were fabricated as previously described.<sup>3,43</sup> The PEGylated GNS nanoparticles (PEG-GNS) were fabricated by PEG-SH (MW: 5,000 Da, Sigma) dispersed in Milli-Q water dropwise to 4.75 ml GNS nanoparticles at the concentration of  $\sim 1 \times 10^{11}$  nanoparticles/ml in Milli-Q water in a 15 ml-glass test tube while vortexing. The final PEG concentration was varied from 0.01-50 nM. The GNS reaction mixture was then left on a shake plate for 1 hour at room temperature. Excess PEG-SH was removed by 3 times centrifugation at 1000 rpm for 30 mins; each time particles were redispersed in 5 ml Milli-Q water. After the final wash, the particles were re-dispersed in 4.75ml of Milli-Q water to keep the concentration of particles to  $\sim 1 \times 10^{11}$  nanoparticles/ml (1mg GNS/ml). The PEG-GNS nanoparticles were stored in Milli-Q water at 4 $^{\circ}$ C before use.

### Characterization of nanoparticles

Nanoparticles were characterized by scanning electron microscopy (SEM) (JOEL 7200 SEM) and UV-Vis spectroscopy (Molecular Devices Spectramax M5). The particle size was calculated based on SEM images. The shell thickness was estimated based on the images of silica NP and GNS nanoparticles. The size distribution and polydispersity, and zeta potential of nanoparticles were examined by the dynamic light scattering (DLS) using a Malvern Zetasizer Nano ZS (Malvern Instruments Ltd Worcestershire, UK).

The silica particle concentration was calculated based on the average volume of each individual silica particle and silica mass concentration determined by freeze-drying an aliquot of known volume of the stock solutions. The molecular weight and density of the silica particles was assumed to be similar to bulk values. The GNS concentration was estimated based on the quantity of silica nanoparticles assuming no loss of silica nanoparticles during the preparation of GNS nanoparticles.

The PEG surface conjugation was characterized by DLS to determine the PEG thickness and zeta potential. PEG thickness was calculated by subtracting the hydrodynamic diameter of the bare gold nanoshells from the PEGylated nanoshells.

### Stimulation of macrophages

THP-1 cells were initially treated in 96-well plates with 2 µg/ml lipopolysaccharide (LPS) from *Escherichia coli* 0111:B4 (Sigma) for 24 hours at  $1 \times 10^5$  cells/well. Priming with Phorbol-12-myristate-13-acetate (PMA, Sigma) prior to LPS did not show a significant effect on IL-1 $\beta$  secretion (Supplementary Figure 1). They were then co-cultured with different nanoparticles and silica  $\mu$ P (Min-U-Sil 15 silica crystals) in culture medium without FBS for 4 hours before the addition of the FBS to a final concentration of 10%. The morphology of cells was monitored up to 24 h. Supernatants were sampled after 24 hours for enzyme-linked Immunosorbent Assay (ELISA). THP-1 cells treated with LPS and incubated with cell culture media only were used as negative controls to determine the background level of IL-1 $\beta$ .

#### ELISA

The level of IL-1 $\beta$  secreted by macrophages was assessed by ELISA. Anti-human IL-1 $\beta$  (clone CRM56) was used as the capture antibody and biotinylated mouse anti-human IL-1 $\beta$  antibody (clone CRM57) was used as the detection antibody. Samples were diluted at a proper range with the blocking buffer (1% FBS in PBS). The detection range for IL-1 $\beta$  was 8 - 2000 pg/ml. Standard procedures described in eBioscience protocol literature (eBioscience) were used.

#### Assessment of the recruitment of neutrophils in vivo

0 – 10 mg per mouse of particles dispersed in 250 µl of Milli-Q water were administered into 8-10 week old female C57BL/6 mice (Jackson Laboratory) by intraperitoneal (i.p.) injection. 250 µl of 10 mg/ml of Aldohydrogel aluminum hydroxide adjuvant (Alum, Brenntag) and sterile PBS were used as positive and negative controls, respectively. After 16 hours, the mice were euthanized by the inhalation of CO<sub>2</sub>. The peritoneal cavity was lavaged by 5 ml of ice cold PBS containing 1% FBS twice. The lavage was pooled. At least 8 ml of the lavage fluid was collected per sample. 7 ml of the lavage fluids were centrifuged, and cells were collected for the identification of neutrophils and the supernatants were collected for the quantification of IL-1 $\beta$ . The cells were incubated with Fc Block (clone number 93, BD Biosciences and subsequently stained with anti-Lys-6G PE (eBioscience) and anti-Lys-6B.2 (7/4) FITC (Abd Serotec). The percentage and number of neutrophils were analyzed by flow cytometry. Data was analyzed using Flowjo software (Tree Star). All the procedures used in this study complied with federal guidelines and institutional policies, and were approved by the University of Washington Institutional Care and Animal Use Committee.

#### Detection of intracellular ROS

Intracellular ROS generation was assessed using the fluorescent probes 2',7'-dichlorodihydrofluorescein diacetate (H<sub>2</sub>DCFDA) (Sigma Aldrich St. Louis, MO). H<sub>2</sub>DCFDA are cell permeable dyes that become fluorescent following the oxidation by ROS into 2',7'-dichlorofluorescein (DCF).  $1 \times 10^5$  of LPS-treated THP-1 cells in 96-well plate were incubated with 100 µl of 10 µM H<sub>2</sub>DCFDA for 45 min, washed twice carefully with DPBS. Then they were given the indicated concentration of nanoparticles dispersed in media without FBS and 2-ME. ROS levels were monitored for a duration of 2 hours at 490 nm<sup>18</sup>/536 nm (Em) by a SpectraMax M5 plate reader at 37°C.

#### Assessment of scavenging effect of nanoparticles

50 µl of hydrogen peroxide (H<sub>2</sub>O<sub>2</sub>, 30%) diluted to 0.2-20 µM was added to 50 µl of sterile-filtered PBS containing GNS and PEG-GNS for 30 min at a final concentration range from 0.1 to 10 µM of H<sub>2</sub>O<sub>2</sub> in 96 well U-bottom plates. The solutions were then spun down at 2000 rpm for 10 min at 4°C to remove all the nanoparticles. 50 µl of the supernatant was then transferred to an opaque white Costar 96-well plate, and mixed with 50 µl of solution containing 10 µM of DCF and 1:100 (v:v) of HRP in sterile filtered PBS. The solutions were allowed to react for 15 min at room temperature before the fluorescence was measured at 490 nm<sup>18</sup>/536 nm (Em) in 96-well plate on a SpectraMax M5 plate reader at 25°C.

#### Assessment of the quenching of fluorescence of DCF by Au nanoparticles

A 50 µl of solution containing 100 µM of H<sub>2</sub>O<sub>2</sub>, HRP at a 1:100 (v:v) ratio, and 10 µM of DCF dispersed in sterile filtered PBS was reacted for 15 min, and then was mixed with 50 µl of nanoparticles in sterile-filtered PBS. The particles were at a final concentration of 0 to 1 mg/ml. The intensity of DCF was measured immediately at 490 nm (Ex)/536 nm (Em) in 96-well plate by a SpectraMax M5 plate reader at 25°C.

#### Statistical analysis

All results are representative of at least three sets of independent experiments, with samples performed in duplicates or triplicates in each experiment. Results represent average values  $\pm$  one standard deviation (SD) of the samples unless otherwise indicated.

## Conclusions

We have demonstrated here that bare Au nanoshell/silica core nanoparticles stimulate the release of the proinflammatory cytokine IL-1 $\beta$  and induced the influx of neutrophils. They join a growing list of particulates that act as "danger signal" and trigger the intracellular sensors of the innate immune system. Colloidal stability of particles in a given physiological environment appears to play a critical role. Aggregations of particles can lead to ROS generation and IL-1 $\beta$  secretions possibly due to frustrated phagocytosis. Surface modification of these particles with PEG can successfully minimize the aggregation and secretion of IL-1. These findings have important implications in designing nanoparticles for either imaging or therapy. Though Au nanoshell/silica core nanoparticles were assessed in this study, our finding that PEGylation reduced the induction of IL-1 $\beta$  and neutrophil influx has implications in other particulates for drug delivery, imaging and therapy as well.

## Acknowledgements

The authors would like to thank Joe Peng for help with the synthesis of PEGylated Au nanoshells, and Lige Tonggu for characterizing nanoparticles by Transmission Electron Microscope. This research was partially supported by the National Science Foundation CAREER Award to H. Shen and the National Institute of Health EB007494 and AI088597 to H.S. The content is solely the responsibility of the authors and does not necessarily represent the official views of NIAID, ORWH or NIH.

## Notes and references

- P. K. Jain, X. H. Huang, I. H. El-Sayed and M. A. El-Sayed, *Accounts of Chemical Research*, 2008, **41**, 1578-1586.
- A. M. Gobin, M. H. Lee, N. J. Halas, W. D. James, R. A. Drezek and J. L. West, *Nano Letters*, 2007, **7**, 1929-1934.
- L. R. Hirsch, R. J. Stafford, J. A. Bankson, S. R. Sershen, B. Rivera, R. E. Price, J. D. Hazle, N. J. Halas and J. L. West, *Proceedings of the National Academy of Sciences of the United States of America*, 2003, **100**, 13549-13554.
- D. P. O'Neal, L. R. Hirsch, N. J. Halas, J. D. Payne and J. L. West, *Cancer Letters*, 2004, **209**, 171-176.
- J. M. Stern, J. Stanfield, W. Kabbani, J. T. Hsieh and J. R. A. Cadeddu, *Journal of Urology*, 2008, **179**, 748-753.
- W. D. James, L. R. Hirsch, J. L. West, P. D. O'Neal and J. D. Payne, *Journal of Radioanalytical and Nuclear Chemistry*, 2007, **271**, 455-459.
- E. S. Day, J. G. Morton and J. L. West, *Journal of Biomechanical Engineering-Transactions of the Asme*, 2009, **131**, 074001-1-5.
- T. A. Erickson and J. W. Tunnell, in *Nanotechnologies for the Life Sciences*, Wiley-VCH Verlag GmbH & Co. KGaA, 2007, DOI: 10.1002/9783527610419.ntls0150.
- S. Lal, S. E. Clare and N. J. Halas, *Accounts of Chemical Research*, 2008, **41**, 1842-1851.
- C. Dostert, V. Petrilli, R. Van Bruggen, C. Steele, B. T. Mossman and J. Tschopp, *Science*, 2008, **320**, 674-677.
- V. Hornung, F. Bauernfeind, A. Halle, E. O. Samstad, H. Kono, K. L. Rock, K. A. Fitzgerald and E. Latz, *Nature Immunology*, 2008, **9**, 847-856.
- T. Morishige, Y. Yoshioka, H. Inakura, A. Tanabe, X. L. Yao, S. Narimatsu, Y. Monobe, T. Imazawa, S. Tsunoda, Y. Tsutsumi, Y. Mukai, N. Okada and S. Nakagawa, *Biomaterials*, 2010, **31**, 6833-6842.
- F. Martinon, V. Petrilli, A. Mayor, A. Tardivel and J. Tschopp, *Nature*, 2006, **440**, 237-241.
- L. Franchi, T. Eigenbrod, R. Munoz-Planillo and G. Nunez, *Nature Immunology*, 2009, **10**, 241-247.
- K. Schroder and J. Tschopp, *Cell*, 2010, **140**, 821-832.
- M. Haruta and M. Daté, *Applied Catalysis A: General*, 2001, **222**, 427-437.
- M. D. Howard, M. Jay, T. D. Dziublal and X. L. Lu, *J. Biomed. Nanotechnol.*, 2008, **4**, 133-148.
- Arnida, A. Malugin and H. Ghandehari, *J Appl Toxicol*, 2010, **30**, 212-217.
- D. Marsh, R. Bartucci and L. Sportelli, *Biochim. Biophys. Acta-Biomembr.*, 2003, **1615**, 33-59.
- B. E. Brinson, J. B. Lassiter, C. S. Levin, R. Bardhan, N. Mirin and N. J. Halas, *Langmuir*, 2008, **24**, 14166-14171.
- A. M. Gobin, J. J. Moon and J. L. West, *INT J NANOMED*, 2008, **3**, 351-358.
- N. Harris, M. J. Ford and M. B. Cortie, *Journal of Physical Chemistry B*, 2006, **110**, 10701-10707.
- X. H. Huang, P. K. Jain, I. H. El-Sayed and M. A. El-Sayed, *Photochem. Photobiol.*, 2006, **82**, 412-417.
- C. Loo, A. Lowery, N. Halas, J. West and R. Drezek, *Nano Letters*, 2005, **5**, 709-711.
- S. J. Oldenburg, J. B. Jackson, S. L. Westcott and N. J. Halas, *Applied Physics Letters*, 1999, **75**, 2897-2899.
- O. Lunov, T. Syrovets, C. Loos, G. U. Nienhaus, V. Mailander, K. Landfester, M. Rouis and T. Simmet, *Acs Nano*, 2011, **5**, 9648-9657.
- D. Perregaux and C. A. Gabel, *J BIOL CHEM*, 1994, **269**, 15195-15203.
- A. M. Nour, Y. G. Yeung, L. Santambrogio, E. D. Boyden, E. R. Stanley and J. Brojatsch, *Infect. Immun.*, 2009, **77**, 1262-1271.
- L. M. Thomas and R. D. Salter, *Journal of Immunology*, 2010, **185**, 3740-3749.
- E. K. Park, H. S. Jung, H. I. Yang, M. C. Yoo, C. Kim and K. S. Kim, *Inflamm. Res.*, 2007, **56**, 45-50.
- G. Y. Chen and G. Nunez, *Nat. Rev. Immunol.*, 2010, **10**, 826-837.
- P. Diagaradjane, A. Shetty, J. C. Wang, A. M. Elliott, J. Schwartz, S. Shentu, H. C. Park, A. Deorukhkar, R. J. Stafford, S. H. Cho, J. W. Tunnell, J. D. Hazle and S. Krishnan, *Nano Letters*, 2008, **8**, 1492-1500.
- R. B. Zhou, A. Tardivel, B. Thorens, I. Choi and J. Tschopp, *Nature Immunology*, 2010, **11**, 136-140.
- I. Nanospectra Biosciences, Pilot Study of AuroLase(tm) Therapy in Refractory and/or Recurrent Tumors of the Head and Neck, <http://clinicaltrials.gov/show/NCT00848042>, (accessed 2012 Sep 22).
- L. R. Hirsch, J. B. Jackson, A. Lee, N. J. Halas and J. West, *Analytical Chemistry*, 2003, **75**, 2377-2381.
- J. Tschopp and K. Schroder, *Nat. Rev. Immunol.*, 2010, **10**, 210-215.
- R. Zhou, A. S. Yazdi, P. Menu and J. Tschopp, *Nature*, 2011, **469**, 221-225.
- S. L. Cassel, S. C. Eisenbarth, S. S. Iyer, J. J. Sadler, O. R. Colegio, L. A. Tephly, A. B. Carter, P. B. Rothman, R. A. Flavell and F. S. Sutterwala, *Proceedings of the National Academy of Sciences of the United States of America*, 2008, **105**, 9035-9040.
- L. A. J. O'Neill, *Science*, 2008, **320**, 619-620.
- H. Zhang, D. R. Dunphy, X. Jiang, H. Meng, B. Sun, D. Tarn, M. Xue, X. Wang, S. Lin, Z. Ji, R. Li, F. L. Garcia, J. Yang, M. L. Kirk, T. Xia, J. I. Zink, A. Nel and C. J. Brinker, *Journal of the American Chemical Society*, 2012, **134**, 15790-15804.
- S. I. Grivennikov, F. R. Greten and M. Karin, *Cell*, 2010, **140**, 883-899.
- S. I. Grivennikov and M. Karin, *Current Opinion in Genetics & Development*, 2010, **20**, 65-71.
- W. Stober, A. Fink and E. Bohn, *Journal of Colloid and Interface Science*, 1968, **26**, 62-69.

**Figure Captions**

**Figure 1.** Characterization of nanoparticles. (A) Scanning electron microscopy (SEM) image of silica nanoparticles (silica NP), and Au nanoshell/silica core nanoparticles (GNS). (B) Hydrodynamic diameter of silica NP (indicated as SNP in B), GNS, PEGylated GNS (PEG-GNS) at different concentrations of PEG-SH in the coating reaction (Rxn). (C) Calculated thickness of PEG corona on PEG-GNS at different concentrations of PEG-SH in the coating reaction. (D) Zeta Potential of nanoparticles. (E) UV-Vis absorption spectra of GNS and 50 nM PEG-GNS in water. The GNS had a surface plasma resonance (SPR) peak at 830 nm. 50 nM PEG-GNS indicates that GNS was coated with PEG at the 50 nM of PEG-SH in the Rxn.

**Figure 2.** Morphology of THP-1 cells incubated with 1 - 5 mg/ml of particles for 1 hour (A) and 4 hours (B) prior to imaging. Images with 1, 3 and 5 mg/ml of GNS (top row) or 50 nM PEG-GNS (middle row) were shown. 50 nM PEG-GNS denotes GNS was coated with PEG at the concentration of 50 nM under experimental conditions. For clarity, Silica NP at 0.1 mg/ml was shown only. Cells with no nanoparticles (Control) were used as controls. Scale bar = 10 $\mu$ m.

**Figure 3.** (A) and (B) IL-1 $\beta$  levels as a function of mass/cell and particles/cell given to THP-1 cells, respectively. LPS-primed THP-1 cells were stimulated with GNS, 50 nM PEG-GNS, and silica NP at concentrations ranging from 0.01 mg/ml to 5 mg/ml. Silica NP were used as a positive control, and untreated cells were used as a negative control (Control). IL-1 $\beta$  secreted by stimulated THP-1 cells were collected after 24 hours and quantified by ELISA. (C) IL-1 $\beta$  level as a function of PEG coverage on GNS represented by the concentration of PEG-SH used in the coating reaction. 3 mg/ml GNS was pegylated with a range of concentrations (0 - 10nM) during the coating reaction. \* indicates  $p < 0.05$  with respect to 0 mg/ml GNS, # indicates  $p < 0.05$  with respect to unpegylated GNS. Values are representative of three independent experiments.

**Figure 4.** (A) Identification of neutrophils by flow cytometry. (B) *In vivo* neutrophil influx assessed for GNS (1, 5, and 10 mg/mouse) and PEG-GNS fabricated at 0.01 and 5 nM PEG-SH at 10 mg/mouse. PBS was used as a negative control. Experiments are representative of three independent experiments. Values are mean  $\pm$  S.D. \* indicates  $p < 0.05$  with respect to PBS control. # indicates  $p < 0.05$  with respect to 10 mg GNS. Values are representative of three independent experiments.

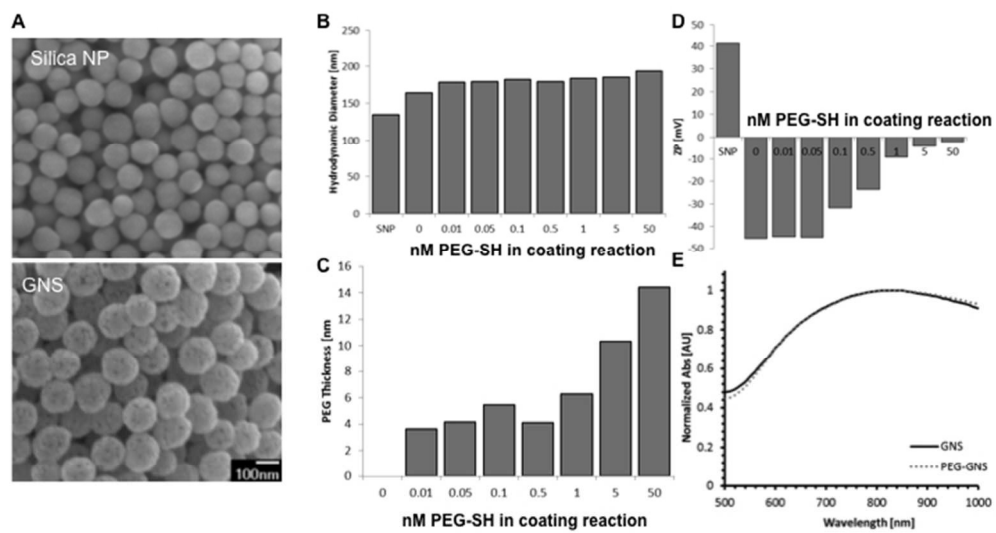
**Figure 5.** Kinetics of ROS generation by THP-1 cells treated with GNS (A), 50 nM PEG-GNS (B), silica NP and microparticles ( $\mu$ P) (C), and H<sub>2</sub>O<sub>2</sub> (D). RFU indicates relative fluorescent units. For clarity, different ranges of fluorescence intensity (DCF RFU), A (0 ~ 200), B (0 ~ 600), C (0 ~ 600), and D (0 ~ 2500), were plotted. The fluorescent intensity of DCF at 60 min was plotted in (E). LPS-treated THP-1 macrophage cells were stimulated with nanoparticles at concentrations ranging from 0.1 mg/ml to 5 mg/ml. Silica NP and  $\mu$ P and extracellular H<sub>2</sub>O<sub>2</sub> were used as a positive control, and untreated cells were used as a negative control (Control). ROS generation was monitored for the duration of 300 min.

**Figure 6.** Scavenging effects of GNS (A) and 50 nM PEG-GNS (B) nanoparticles. Values were subtracted from PBS samples with the addition of nanoparticles but without H<sub>2</sub>O<sub>2</sub>. Values are mean  $\pm$  S.D. \* indicates  $p < 0.05$  with respect to samples without nanoparticles. Values are representative of three independent experiments.

**Figure 7.** Quenching effects of GNS (A) and 50nM PEG-GNS (B) nanoparticles. Values are mean  $\pm$  S.D. \* indicates  $p < 0.05$  with respect to

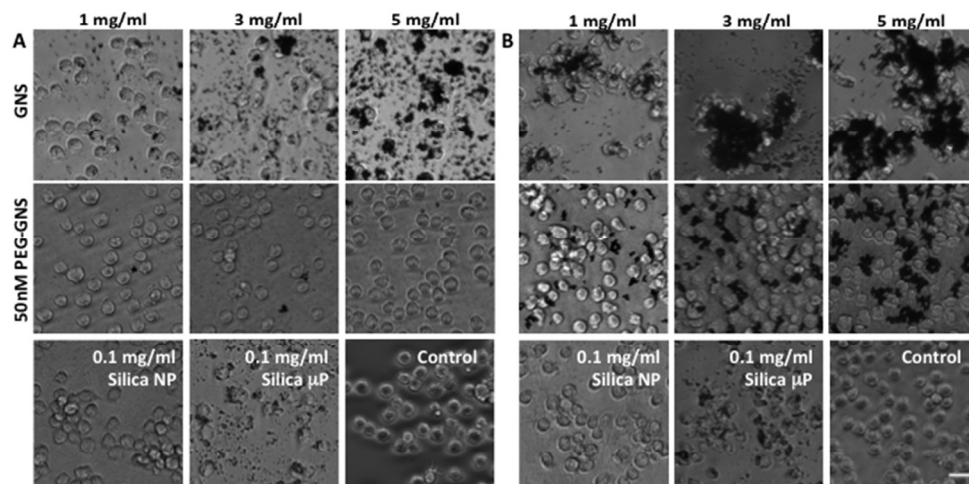
controls without nanoparticles. Values are representative of three independent experiments.

Figure 1



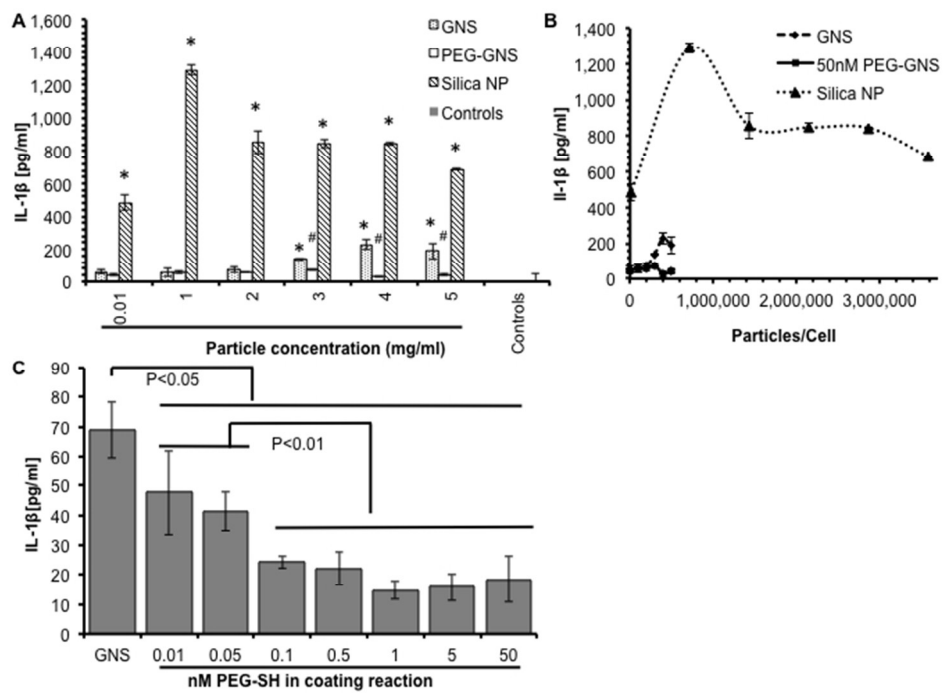
254x190mm (72 x 72 DPI)

Figure 2



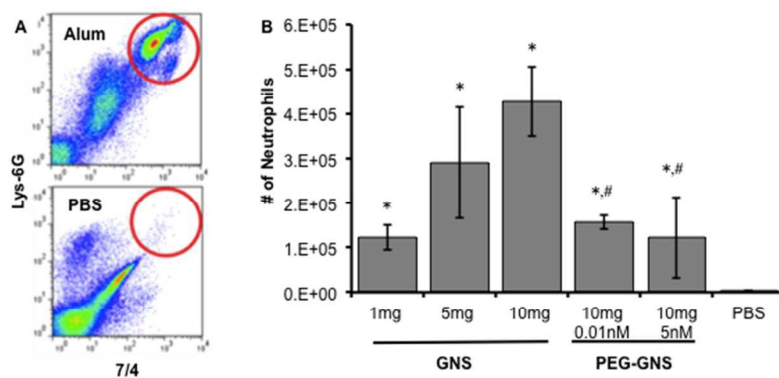
254x190mm (72 x 72 DPI)

Figure 3



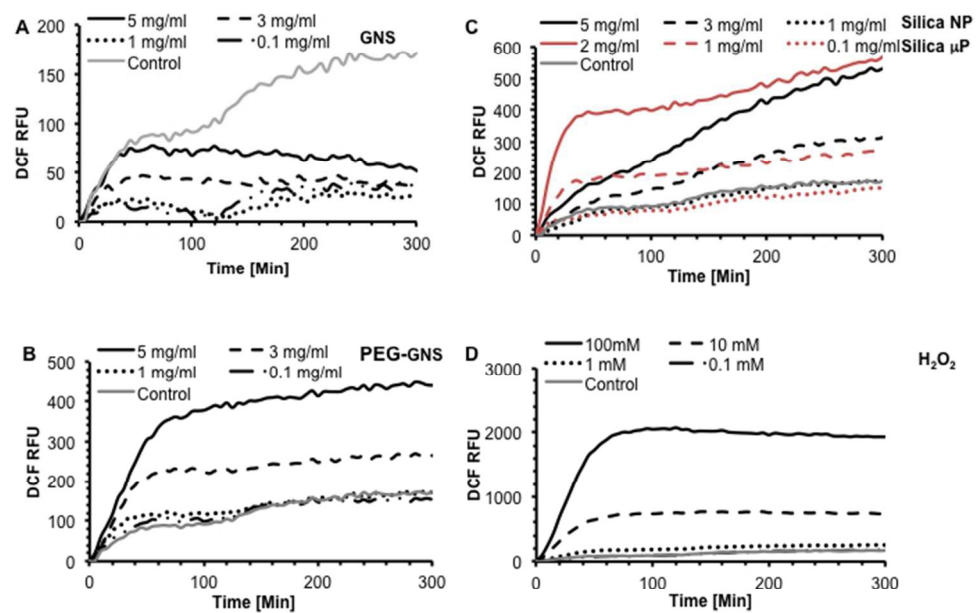
254x190mm (72 x 72 DPI)

Figure 4

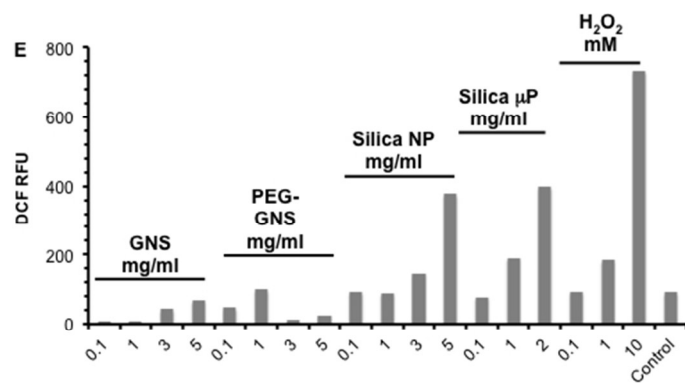


254x190mm (72 x 72 DPI)

Figure 5

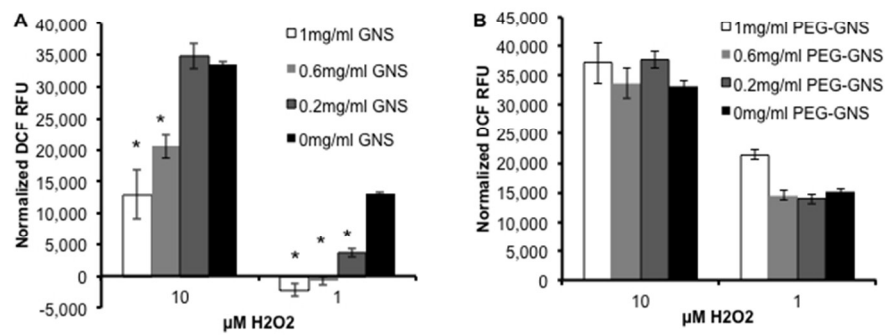


254x190mm (72 x 72 DPI)

Figure 5  
Continued

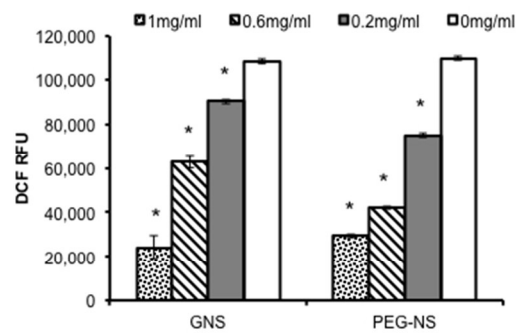
254x190mm (72 x 72 DPI)

Figure 6



254x190mm (72 x 72 DPI)

Figure 7



254x190mm (72 x 72 DPI)

PEGylation of Au nanoshell/silica core (GNS) particles reduces the aggregation in cell culture and the generation of IL-1 $\beta$  and the influx of neutrophils in mouse peritoneal cavity.

